Azimuth-Track-Level Compensation to Reduce Blind-Pointing Errors of the Beam-Waveguide Antennas

W. Gawronski[1], F. Baher[1], and O. Quintero[2]

The deviations of the azimuth track level of a beam-waveguide (BWG) antenna shall not exceed ±0.5 mm. During tracking, this amplitude of deviations causes deformations of antenna structure, resulting in pointing errors that exceed the required accuracy for 32-GHz (Ka-band) tracking. However, structural deformations caused by the azimuth-track unevenness are repeatable; therefore, a look-up table can be created to improve the blind-pointing accuracy. This article presents the process for creation of the look-up table, describes the instrumentation (inclinometers and data-collection system) necessary for determining the pointing errors, and describes the processing of inclinometer data. It derives algorithms for the pointing-error estimation and for the azimuth-axis tilt using the inclinometer data. It compares the error corrections based on the created look-up table and actual measurements of pointing errors using the conical scanning (CONSCAN) technique. This comparison shows a satisfactory convergence that justifies the implementation of the approach in the forthcoming NASA missions.

I. Introduction

During tracking, an uneven azimuth-track level causes antenna tilts and flexible deformations, which deteriorate pointing accuracy. According to the specification,[3] the level deviations should not exceed ±0.5 mm. Preliminary analysis indicated that this level of deviations could cause pointing errors exceeding the 32-GHz (Ka-band) tracking requirement of 1.5 mdeg. However, the pointing errors caused by the track irregularities are repeatable; therefore, they can be calibrated. By developing a look-up table, one provides pointing corrections as a function of the antenna azimuth position. The look-up table is generated by measuring tilts of the alidade structure at selected points. The effectiveness of this procedure is ultimately checked by the measurement of the antenna pointing error during tracking. In 1997, at the James Clerk Maxwell Telescope in Hawaii, a loop-up table that compensates for the track-level unevenness was tested and implemented (see www.jach.hawaii.edu/JACpublic/JCMT/pointing/inclinometry.html). However, the amount of pointing improvement has not been published.

---

[1] Communications Ground Systems Section.

[2] Space Instruments Implementation Section.

[3] R. Geisich, *Azimuth Track and Pintle Bearing Installation, Alignment, and Grounding*, JPL IP 515904 (internal document), Jet Propulsion Laboratory, Pasadena, California, June 14, 1994.

The task of blind-pointing-error correction due to track-level unevenness consists of the following steps, described subsequently in this article:

(1) Carry out finite-element analysis of the alidade structure to select inclinometer locations.

(2) Develop algorithms to determine the (a) pointing errors, (b) azimuth-axis tilt, and (c) azimuth-track profile from inclinometer data.

(3) Choose the optimal azimuth rate for data collection, collecting data and verifying the pointing model through the antenna wheel shimming.

(4) Process data, checking repeatability and smoothing the data.

(5) Create the look-up table.

(6) Verify the blind-pointing-error correction table using conical scanning (CONSCAN).

II. Hardware and Software Description

Hardware components of the track-level-compensation (TLC) system consist of eight inclinometers, an interface assembly, an industrial PC computer, and several single-based computer boards (analog-to-digital converter and digital input–output data-acquisition boards). The communication between the different components of the system is through parallel port (see Fig. 1).

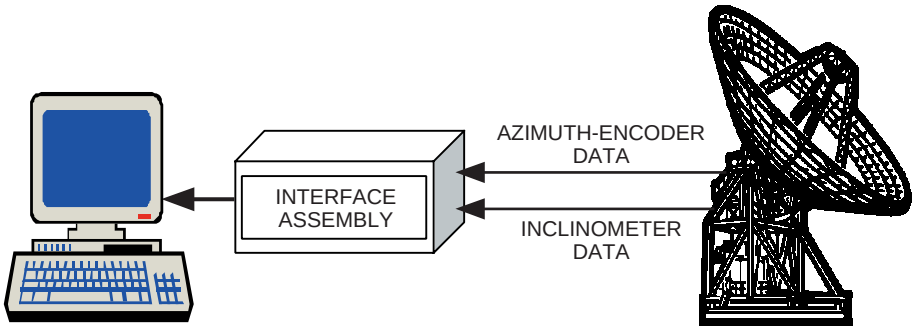

Fig. 1. Block diagram of the track-level data-collection system.

Eight surface-mount inclinometers, Model 711-2 from Applied Geomechanics, are mounted at the antenna. These low-power, dual-axis, analog-output inclinometers contain temperature sensors. The calibration procedure of the inclinometers is described in detail in [3]. The best calibration results are obtained in a uniform temperature distribution on the antenna surface, observed after sunset. The output scale factors of the inclinometer are selected using the low-gain no-filter mode and by measuring the output in a differential mode.

Data were collected at the high-gain and no-filter mode. The output scale factor for the differential mode was determined according to the procedure in [3] and was different for each inclinometer.

The interface box is used to process the inclinometer and antenna azimuth-encoder data to the format acceptable by a PC computer. The data are collected via A/D and digital I/O boards installed in the computer. These single-based computer boards allow for the recording of the inclinometers and azimuth-encoder data.

The software components of the system include Windows NT (real-time operations), Labview (an instrumentation and graphical program), and Matlab (an analysis tool). The data were monitored and collected using Labview and were post-processed and analyzed by Matlab.

III. Inclinometer Data

Eight inclinometers were installed on the alidade structure, and their locations are marked in Fig. 2. Each inclinometer measures tilts of its x- and y-axes. The locations of the inclinometers were selected using the finite-element analysis of the alidade structure. The inclinometers are located such that their tilts can be used to estimate the alidade elevation and cross-elevation rotations next to the antenna focal point. Inclinometers 1 and 2 are located at the top of the alidade. Inclinometer 2 is located next to the elevation encoder. Thus, the y-axis tilt of this inclinometer reflects the elevation pointing error. Inclinometers 7 and 8 are located in the middle of the cross beam of the left and right sides of the alidade, respectively. Their x-axis tilts, combined with the x-axis tilts of inclinometers 1 and 2, give the cross-elevation pointing error, as will be shown later in this article. Inclinometers 3 through 6 are used for checking the accuracy of the cross-elevation-error model and also for determining the azimuth-track profile. The following notation is used: the x- and y-axis tilts of the ith inclinometer are denoted α_{ix} and α_{iy}, respectively.

The inclinometer data were collected during the antenna azimuth rotation with a constant rate of 50 mdeg/s at the sampling frequency of 2 Hz. The rate of 50 mdeg/s was selected after testing different rates and measuring the noise-level, temperature-gradient impact (through repeatability of the data). Low-rate data have lower noise levels but larger repeatability errors than high-rate data. The tests were performed during nighttime to minimize distortions of the antenna structure due to the thermal

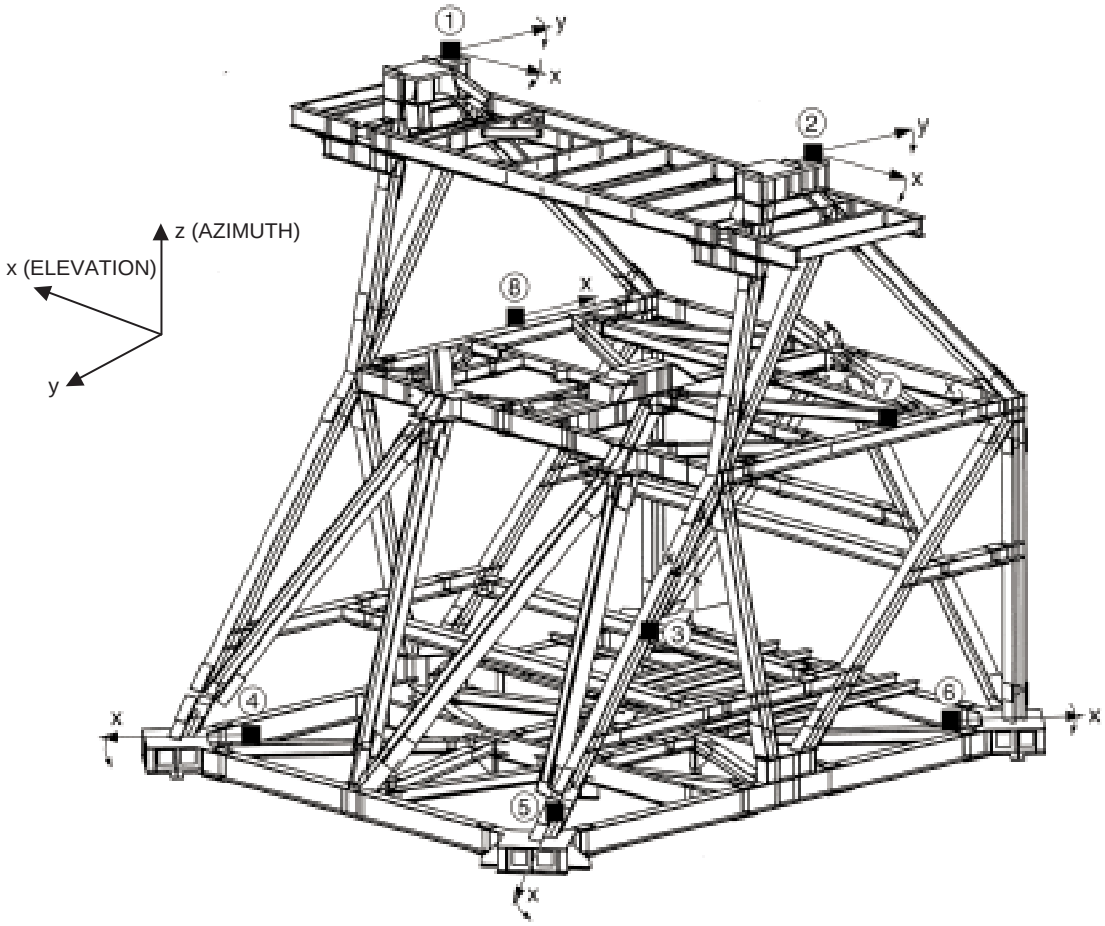

Fig. 2. Inclinometer locations on the alidade structure.

gradient. We collected six sets of data for full (0 to 360 deg) azimuth rotations, four for the clockwise rotations, and two for the counterclockwise rotations. The data show satisfactory repeatability in the clockwise direction (see Figs. 3 through 5). There are some drifts due to other factors, such as temperature variations; there was about a 3-hour shift between each data collection at night. The alidade deformation due to temperature drift was recorded while the antenna was stowed. A sample of the inclinometer data is shown in Fig. 6. From this figure, one can see that, within the time span of 3 hours, the temperature change causes the inclinometer to drift about 0.5 mdeg.

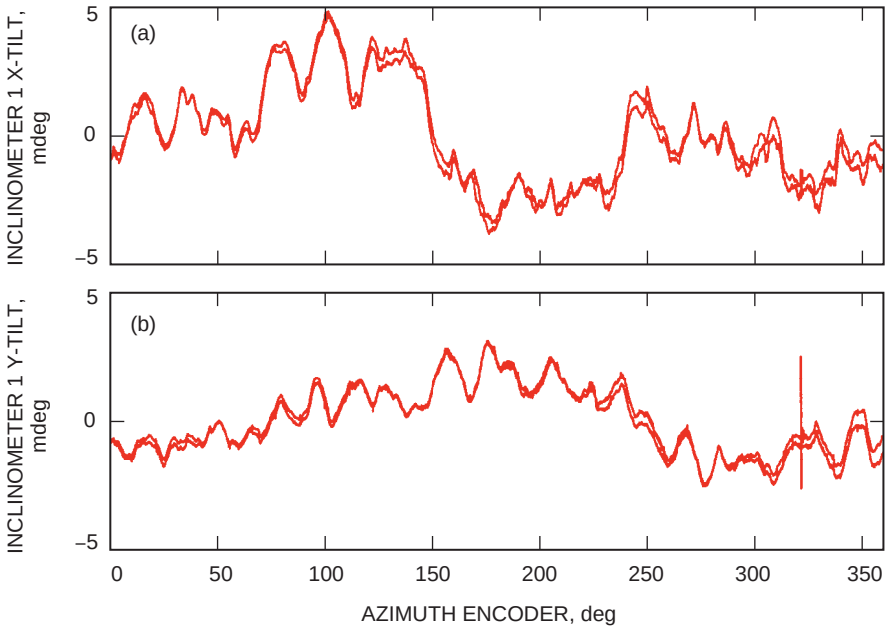

Fig. 3. Repeatability of inclinometer 1 readings: (a) x-tilt and (b) y-tilt.

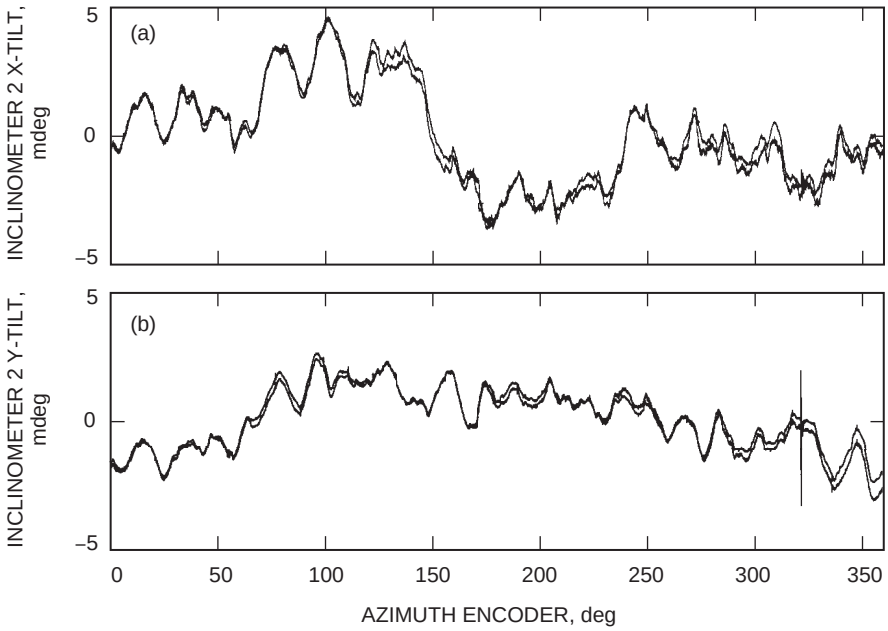

Fig. 4. Repeatability of inclinometer 2 readings: (a) x-tilt and (b) y-tilt.

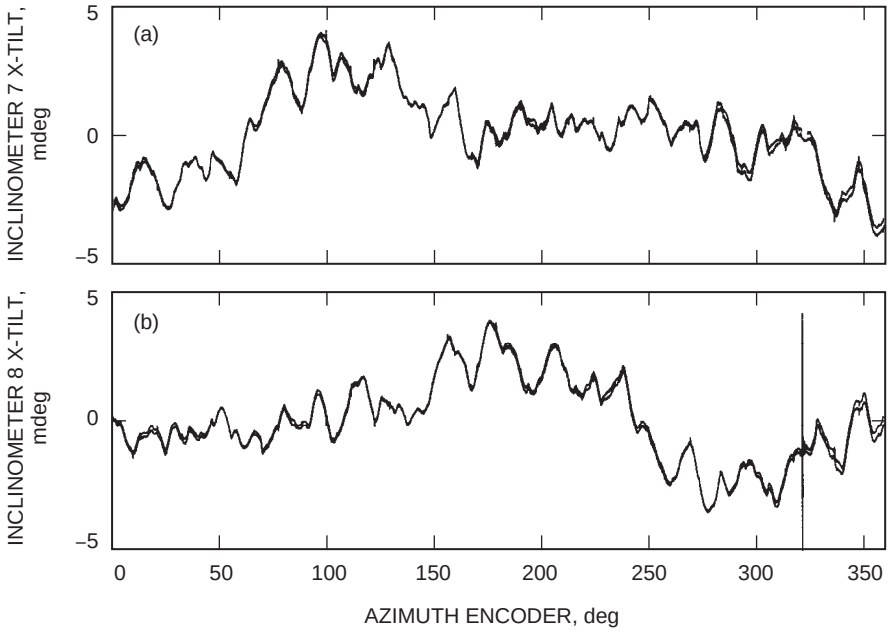

Fig. 5. Repeatability of inclinometer x-tilt readings: (a) inclinometer 7 and (b) inclinometer 8.

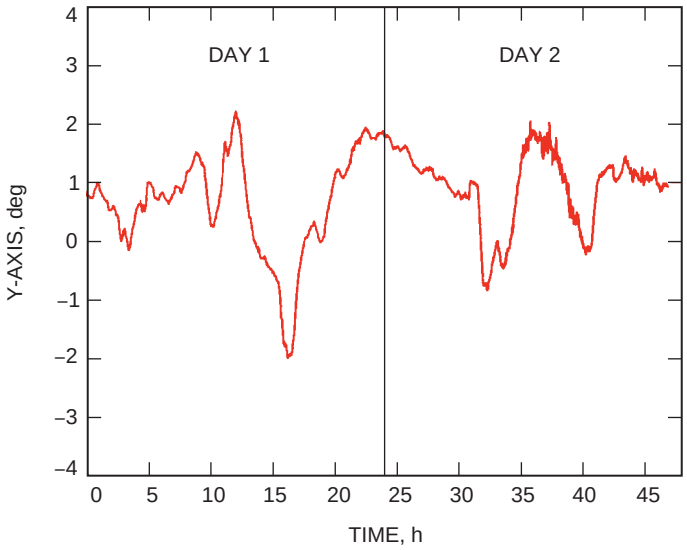

Fig. 6. The y-tilt of inclinometer 1 due to the thermal deformations of the alidade.

Do the errors caused by the azimuth-track unevenness depend on the antenna elevation position? This question was answered by collecting data for the antenna elevation angles of 15, 45, 60, and 89 deg. All inclinometer readings were the same (within the instrument accuracy), showing that the azimuth-track-profile pointing errors do not depend on the antenna elevation position.

The data were smoothed using a zero-phase lowpass filter (see, for example, [1]), using the Matlab *filtfilt* routine [2]. This filter smoothes the data without shifting them. The longer the averaging, the smoother the curve. It was determined that a length of 50 smoothes small "bumps" that are undesirable in the look-up table.

IV. Determining Pointing Errors

The y-tilt of the second inclinometer is a rotation with respect to the antenna x-axis, denoted δ_x. It is a measure of the antenna elevation error, Δ_{el}:

$$\Delta_{el} = \delta_x = \alpha_{2y} \tag{1}$$

[see Fig. 7(a)].

The cross-elevation error, Δ_{xel}, depends on the antenna elevation position, θ_{el}. It depends also on the rotation, δ_y, of the top of the alidade with respect to the y-axis (tilt of the elevation axis) and the alidade twist, δ_z (the rotation of the top of the alidade with respect to the z-axis):

$$\Delta_{xel} = \delta_z \cos(\theta_{el}) - \delta_y \sin(\theta_{el}) \tag{2}$$

[see Fig. 7(b)]. The orientation of axes x, y, and z with respect to the antenna dish is described in Fig. 8.

The tilt of the elevation axis is an average of the x-tilts of inclinometers 1 and 2, that is,

$$\delta_y = 0.5(\alpha_{1x} + \alpha_{2x}) \tag{3}$$

while the alidade twist is not directly measured by inclinometers. It is determined from the x-tilts of inclinometers 7 and 8 by assuming that the y-tilt of the side inclinometers (7 and 8) is a satisfactory measure of the horizontal displacements of the top of the antenna. Based on this assumption, the following estimate of the antenna twist was obtained (see Appendix A):

$$\delta_z = \frac{h(\alpha_{7x} - \alpha_{8x})}{l} \tag{4}$$

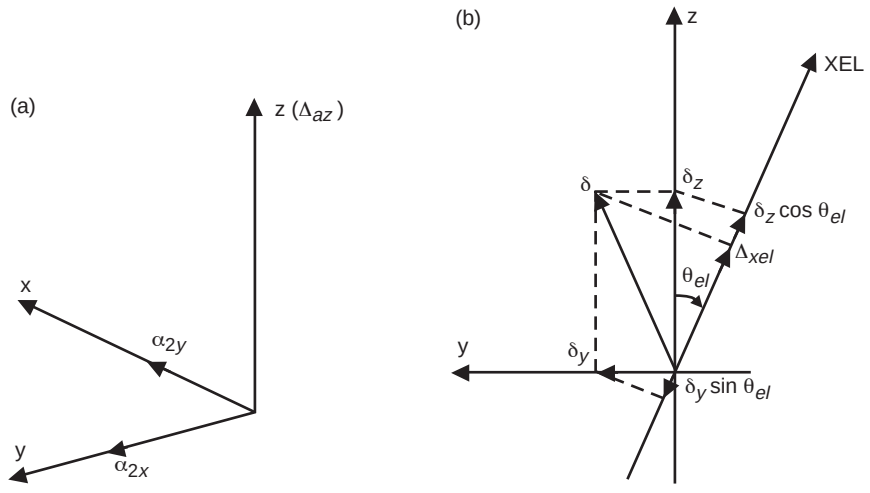

Fig. 7. Inclinometer 2: (a) tilts of the inclinometer and the azimuth correction angle, and (b) the x-, y-, and z-rotations of the alidade, and the cross-elevation correction angle.

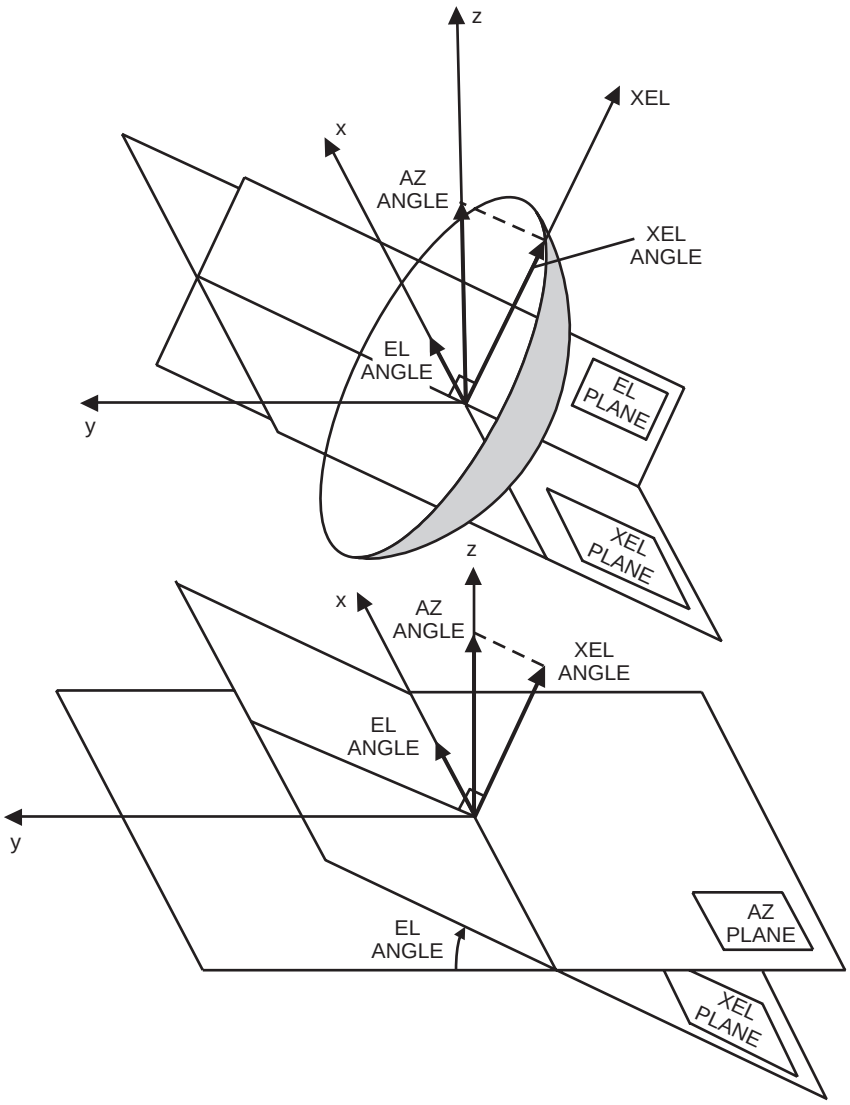

Fig. 8. The relationship between azimuth and cross-elevation errors.

where h is the alidade height and l is the distance between inclinometers 1 and 2 (see Fig. A-1 in Appendix A). Since $h/l = 1.245$, we found that

$$\delta_z = 1.245(\alpha_{7x} - \alpha_{8x}) \tag{5}$$

Combining Eqs. (2), (3), and (5), the cross-elevation pointing error is determined from the x-tilts of inclinometers 1, 2, 7, and 8 as follows:

$$\Delta_{xel} = 1.245(\alpha_{7x} - \alpha_{8x})\cos(\theta_{el}) - 0.5(\alpha_{1x} + \alpha_{2x})\sin(\theta_{el}) \tag{6}$$

The azimuth error is a function of the cross-elevation error,

$$\Delta_{az} = \frac{\Delta_{xel}}{\cos(\theta_{el})} \tag{7}$$

Therefore,

$$\Delta_{az} = \delta_z - \delta_y \tan(\theta_{el}) \tag{8}$$

or

$$\Delta_{az} = 1.245(\alpha_{7x} - \alpha_{8x}) - 0.5(\alpha_{1x} + \alpha_{2x}) \tan(\theta_{el}) \tag{9}$$

The accuracy of the assumption of using side inclinometers as estimators of the horizontal displacements of the alidade top is checked using the inclinometer field data (see Fig. 9). In these figures, the plots of the top, middle, and bottom tilts of the alidade sides were determined. The first two were directly measured by inclinometers 1, 2, 7, and 8; the bottom tilt was derived from x-tilts of inclinometers 3 through 6. The antenna shimming, as described in the following section, relates the x-tilts of inclinometers 3 through 6 to the wheel (or lower beam-end) displacement. The difference between the beam-end displacements divided by the beam length gives the lower-beam tilt. These tilts show flexible deformations on top of the rigid-body motion (for pure rigid-body motion, these three angles would be identical). The middle-beam angle was chosen as an estimator of the top horizontal displacement. Its accuracy can be verified through the averaging of the rotations of the top and the bottom locations. Figure 10 shows satisfactory convergence between the middle-beam rotation and the average rotation of the bottom and the top locations.

The δ_x, δ_y, and δ_z alidade rotations were smoothed for azimuth angles varied from 0 to 360 deg for a 0.1-deg azimuth-angle sample size. Their plots are shown in Fig. 11. These three plots are used for the error correction in Eqs.(1) and (2).

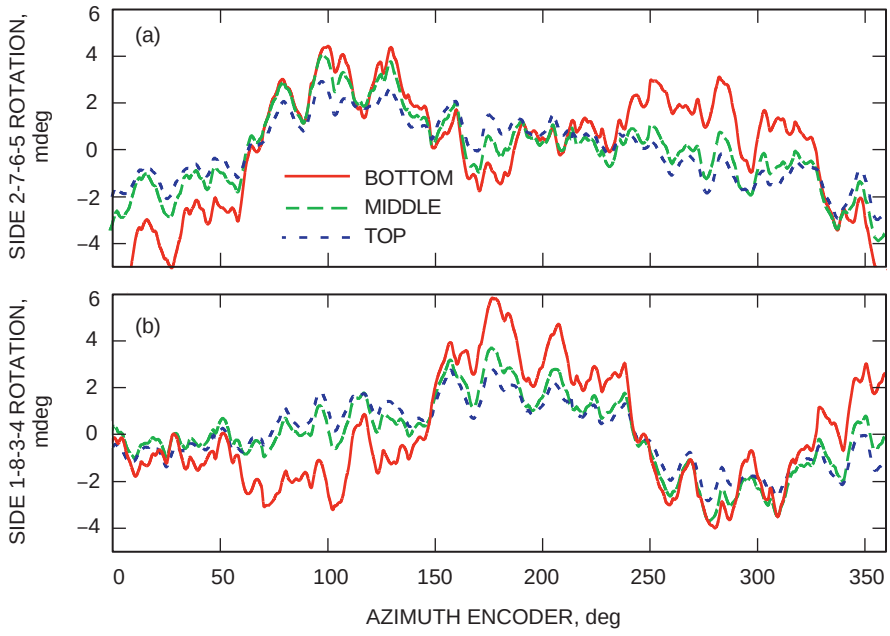

Fig. 9. Rotations of the alidade: (a) 2-7-6-5 side and (b) 1-8-3-4 side.

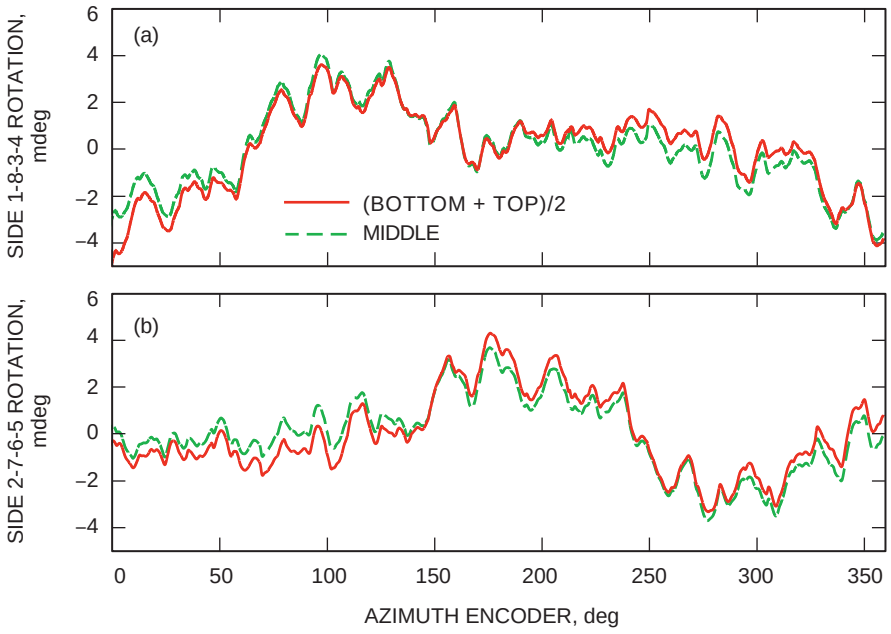

Fig. 10. Rotations of the (a) 1-8-3-4 and (b) 2-7-6-5 middle bars of the alidade, and the average rotation of the alidade.

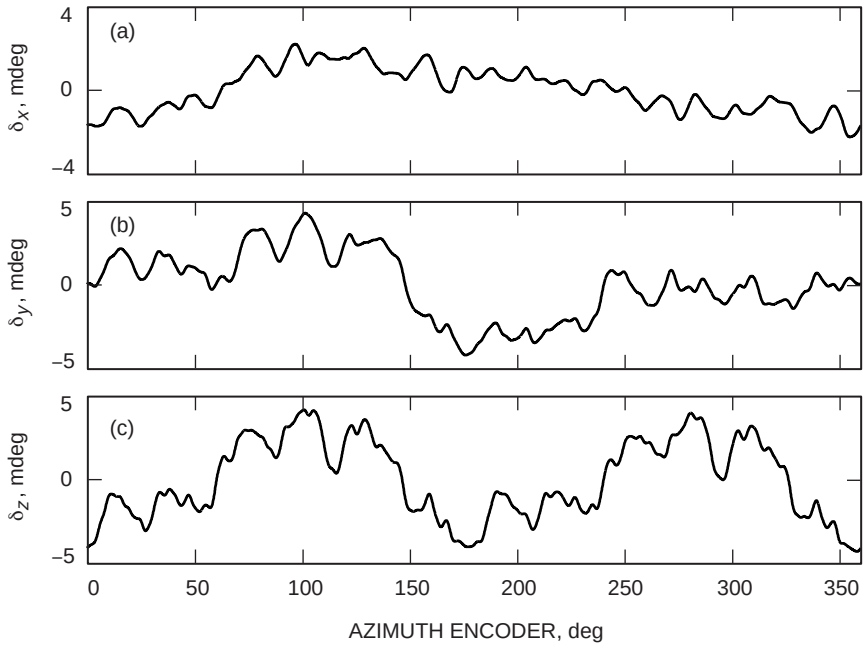

Fig. 11. Rotations of the alidade due to azimuth-track unevenness: (a) x-rotation (b) y-rotation, and (c) z-rotation.

V. Determining the Track Profile

The wheel shimming and tilt measurements were conducted to show the relationship between the inclinometer tilt and the azimuth-track unevenness. For inclinometers 3 through 6, it was a 14.8-mdeg x-tilt for the 2.5-mm of wheel lift. Based on this scaling and the continuous records of the lower inclinometer x-tilt measurements during the antenna constant-rate slewing, the azimuth-track profile was determined and is shown in Fig. 12. It is seen from this figure that the maximum peak-to-peak track-profile variation is 1.22 mm, slightly higher than the specification (1.02 mm).[4]

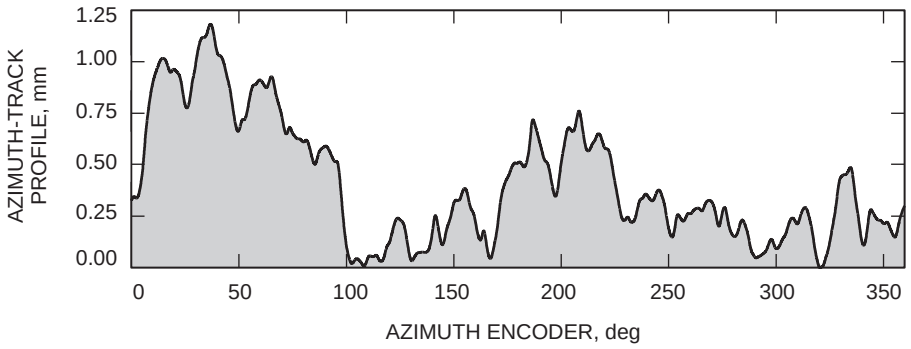

Fig. 12. Azimuth-track-unevenness profile.

VI. Determining the Azimuth-Axis Tilt

Using the inclinometer data, one can determine the azimuth-axis tilt. It is represented as a sinusoidal component in the inclinometer measurements. Its amplitude, a, and phase, φ, need to be determined. Let $\alpha_{1x}(i)$ and $\alpha_{1y}(i)$ be the ith sample of the x- and y-tilts, respectively, of inclinometer 1 and $e(i)$ be the ith sample of the azimuth encoder. The inclinometer harmonics caused by the azimuth-axis tilt are described as

$$\left.\begin{aligned} \alpha_{1x}(i) &= a\cos(e(i)+\varphi) \\ \alpha_{1y}(i) &= a\sin(e(i)+\varphi) \end{aligned}\right\} \tag{10}$$

The amplitude and phase of the tilt are determined as follows (for the derivation, see Appendix B):

$$\left.\begin{aligned} a &= \sqrt{A_{11}^2 + A_{21}^2} \\ \varphi &= \tan^{-1}\left(\frac{A_{21}}{A_{11}}\right) \end{aligned}\right\} \tag{11}$$

where $A = \left\{ \begin{matrix} A_{11} \\ A_{21} \end{matrix} \right\}$ is obtained from the following equation:

$$A = (P^T P)^{-1} P^T \alpha_1 \tag{12}$$

[4] Ibid.

In this equation,

$$\alpha_1 = \left\{ \begin{array}{c} \alpha_{1x} \\ \alpha_{1y} \end{array} \right\} \tag{13a}$$

where $\alpha_{1x} = \left\{ \begin{array}{c} \alpha_{1x}(1) \\ \alpha_{1x}(2) \\ \vdots \\ \alpha_{1x}(n) \end{array} \right\}$ and $\alpha_{1y} = \left\{ \begin{array}{c} \alpha_{1y}(1) \\ \alpha_{1y}(2) \\ \vdots \\ \alpha_{1y}(n) \end{array} \right\}$, and

$$P = \begin{bmatrix} c & -s \\ s & c \end{bmatrix} \tag{13b}$$

where $c = \left\{ \begin{array}{c} c_1 \\ c_2 \\ \vdots \\ c_n \end{array} \right\}$ and $s = \left\{ \begin{array}{c} s_1 \\ s_2 \\ \vdots \\ s_n \end{array} \right\}$. Based on several sets of data we obtained from Eq. (11), the following are the amplitude and phase of the azimuth-axis tilt:

$$a = 1.6 \text{ mdeg}$$

and

$$\varphi = -64 \text{ deg}$$

The plots of the inclinometer tilts with the best-fit sinusoid of the azimuth-axis tilt are shown in Figs. 13(a) and 14(a). The sinusoid was subtracted from the inclinometer data, and the residuals are shown in Figs. 13(b) and 14(b). They show that, even for the perfectly vertical azimuth axis, the pointing error due to azimuth-track unevenness is 4 to 6 mdeg, peak-to-peak, and it is repeatable.

VII. Verification of the Look-Up Table Using CONSCAN Measurements

On DOY 349 of 1997, CONSCAN pointing errors were measured while continuously tracking a single point source (0927+390) for 8 hours, from 10 p.m. to 6 a.m. local time for azimuth ranges from 305 to 330 and 0 to 50 deg. The CONSCAN-derived pointing errors are shown as dots in Fig. 15, while the inclinometer-derived pointing errors are shown as a solid line. The results show a significant correlation between the CONSCAN- and inclinometer-derived errors. Each data set shows agreement at the sub-millidegree level.

VIII. Conclusions

The alidade three-axis rotation table as a function of the antenna azimuth position was obtained from the measured inclinometer tilts. From this table, the antenna pointing errors were derived. These errors were compared with the CONSCAN-derived errors, showing good coincidence and the potential to reduce the blind pointing by 2 to 3 mdeg. The procedure was designed as a look-up table to compensate for the

azimuth-track-level unevenness. It shows potential as an on-line measuring device to compensate for all errors caused by the alidade tilts (this includes azimuth-track unevenness, azimuth-axis tilt, and thermal deformations).

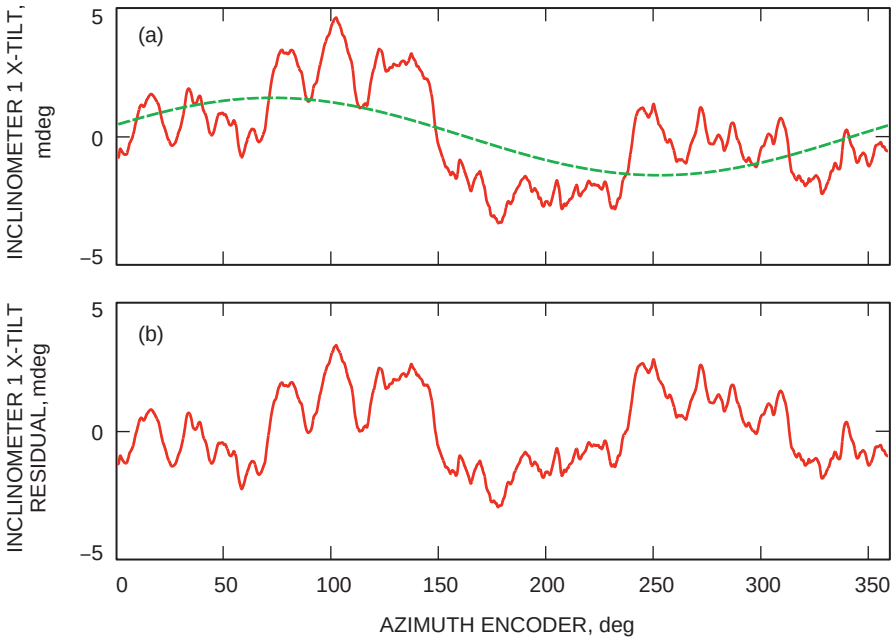

Fig. 13. Inclinometer 1 x-tilt (a) with the azimuth-axis tilt and (b) with the azimuth-axis tilt removed.

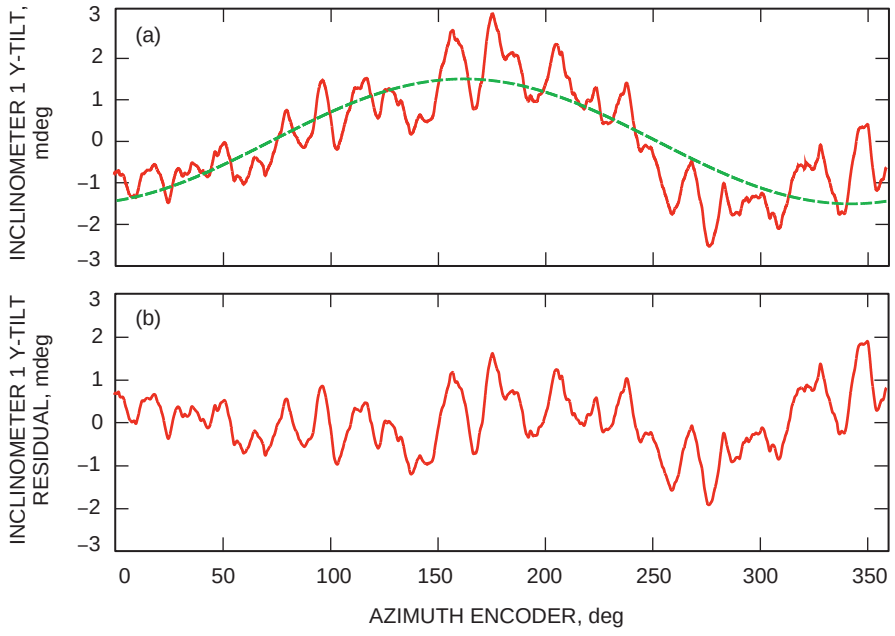

Fig. 14. Inclinometer 1 y-tilt (a) with the azimuth-axis tilt and (b) with the azimuth-axis tilt removed.

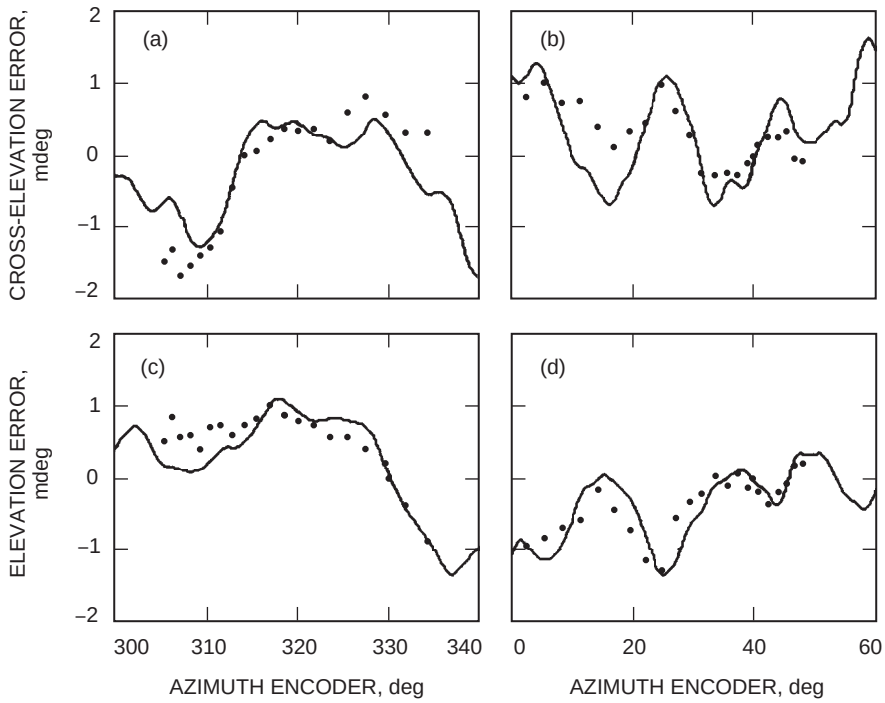

Fig. 15. Pointing errors obtained from the azimuth correction table (solid line) and CONSCAN measurements (dots). Cross-elevation error for azimuth angles from (a) 300 to 340 deg and (b) 0 to 60 deg, and elevation error for azimuth angles from (c) 300 to 340 deg and (d) 0 to 60 deg.

Acknowledgments

The authors would like to thank Chris Yung for recognizing the problem and initializing it and for discussions of technical problems; John Cucchissi and Mark Gatti for technical discussions and leadership; Ian Pain of the James Clerk Maxwell Telescope of Mauna Kea, Hawaii, for advice in the initialization of this research; Paul Richter and David Rochblatt for CONSCAN data collection and discussions that allowed for improvement of this article; Tim Sink for helping in the antenna measurements; and Hal Ahlstrom for discussions that resolved several technical problems.

References

[1] S. D. Stearns and D. R. Hush, *Digital Signal Analysis*, Englewood Cliffs, New Jersey: Prentice Hall, 1990.

[2] *Matlab Signal Processing Toolbox User's Guide*, Version 4, Mathworks, 1996.

[3] *User's Manual: 700-Series Platform and Surface Mount Tiltmeters*, Applied Geomechanics, 1997.

[4] *User's Manual: Model 771 Digital Readout Unit*, Applied Geomechanics, 1988.

Appendix A

Derivation of the Cross-Elevation Pointing Error From the Inclinometer Data

The cross-elevation error, Δ_{xel}, depends on the antenna elevation position, θ_{el}. It depends also on the rotation, δ_y, of the top of the alidade with respect to the y-axis (tilt of the elevation axis) and the alidade twist, δ_z (the rotation of the top of the alidade with respect to the z-axis), i.e.,

$$\Delta_{xel} = \delta_z \cos(\theta_{el}) - \delta_y \sin(\theta_{el}) \tag{A-1}$$

[see Fig. 7(b)].

The tilt of the elevation axis is an average of the x-tilts of inclinometers 1 and 2; that is,

$$\delta_y = 0.5(\alpha_{1x} + \alpha_{2x}) \tag{A-2}$$

while the alidade twist is not directly measured by inclinometers. It is determined as follows. From Fig. A-1,

$$\delta_z = \frac{\Delta x_2 - \Delta x_1}{l} \tag{A-3}$$

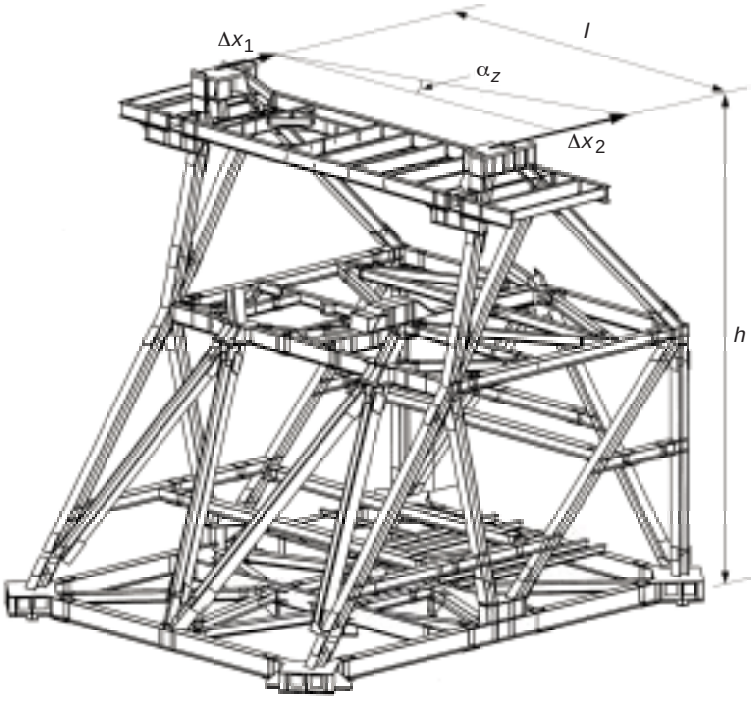

Fig. A-1. Determination of the z-rotation of the alidade.

where Δx_1 and Δx_2 are horizontal displacements of the locations of inclinometers 1 and 2 and $l = 12.40$ m is the distance between the two inclinometers. The displacements, Δx_1 and Δx_2, are determined from the tilts of inclinometers 8 and 7, respectively, by assuming that the horizontal displacement of the alidade side due to azimuth-track unevenness is caused predominantly by the rigid-body motion of each side of the alidade, as shown in Fig. A-2. This assumption was checked with the finite-element model of the alidade (see Fig. A-3). Using the finite-element model, we determined Δx_1 and Δx_2 displacements, assuming the rigid-body rotation of the bottom beam, and compared it with the actual displacements, Δx_1 and Δx_2, that included flexible deformations. The difference was 18 percent with respect to true rotations. If the displacement were determined using the rigid-body assumption and the rotation of the middle beam, the error in Δx_1 and Δx_2 displacements is less than 7 percent. Thus, the middle-beam rotation was selected as a rigid-body rotation estimator. This angle is measured as the x-tilt of inclinometers 7 and 8 (denoted as α_{7x} and α_{8x}, respectively). The top displacements, Δx_1 and Δx_2, of the alidade are obtained from the rigid-body angles as follows, based on the alidade geometry shown in Fig. A-4. From this figure, we have

$$\left.\begin{aligned} \Delta x_o &= s\Delta\alpha \\ \Delta x &= \Delta x_o \cos(\beta) \end{aligned}\right\} \tag{A-4a}$$

Hence,

$$\Delta x = s\,\cos(\beta)\,\Delta\alpha = h\,\Delta\alpha \tag{A-4b}$$

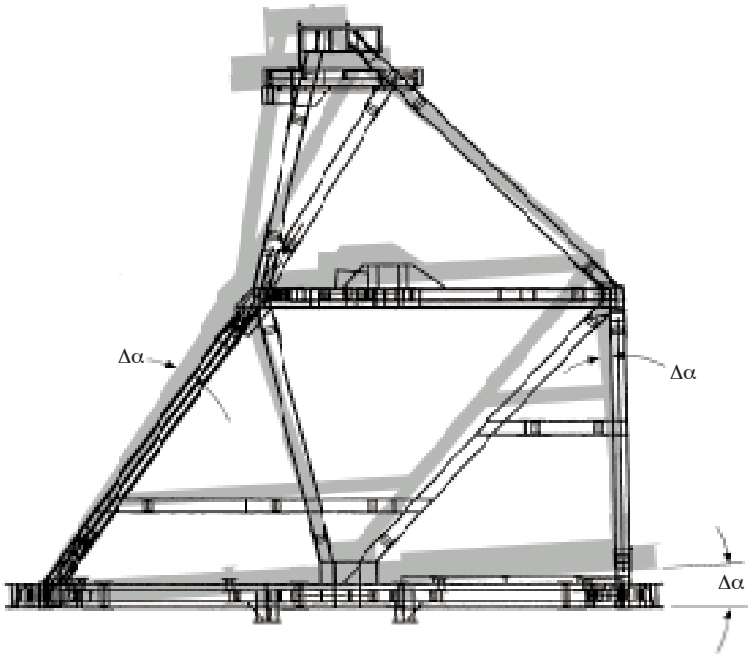

Fig. A-2. Rigid-body rotation of the alidade side.

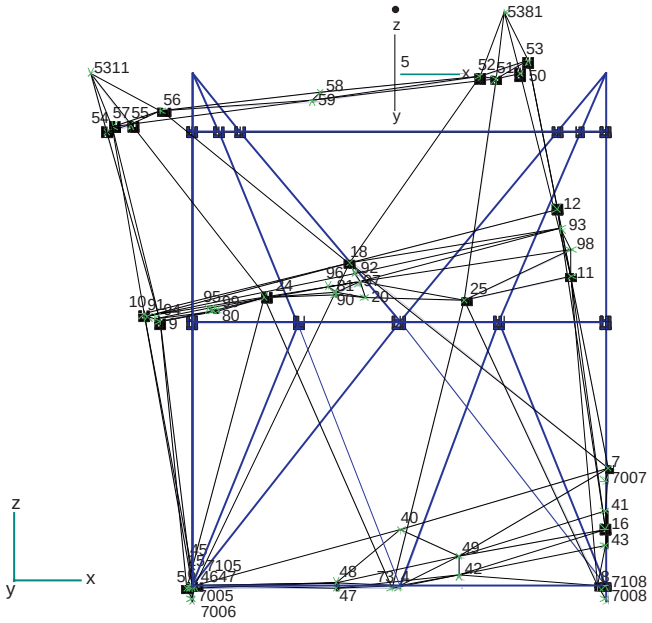

Fig. A-3. Deformation of the alidade due to a single-wheel vertical displacement.

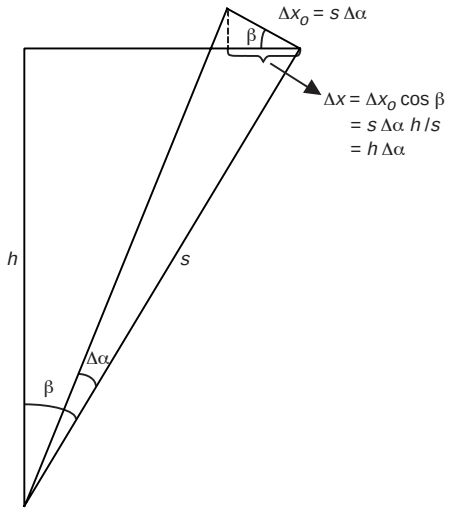

Fig. A-4. Determination of the alidade rotation.

Therefore,

$$\left.\begin{aligned}\Delta x_1 &= h\alpha_{8x}\\ \Delta x_2 &= h\alpha_{7x}\end{aligned}\right\} \tag{A-5}$$

and $h = 15.43$ m.

Introducing Eq. (A-5) to Eq. (A-3), we obtain

$$\delta_z = \frac{h(\alpha_{7x} - \alpha_{8x})}{l} \tag{A-6}$$

or, since $h/l = 1.245$, we found that

$$\delta_z = 1.245(\alpha_{7x} - \alpha_{8x}) \tag{A-7}$$

Combining Eqs. (A-1), (A-3), (A-4), and (A-7), the cross-elevation pointing error and the azimuth error are determined from the x-tilts of inclinometers 1, 2, 7, and 8 as follows:

$$\Delta_{xel} = 1.245(\alpha_{7x} - \alpha_{8x})\cos(\theta_{el}) - 0.5(\alpha_{1x} + \alpha_{2x})\sin(\theta_{el}) \tag{A-8}$$

Appendix B

Derivation of the Azimuth-Axis Tilt From the Inclinometer Data

The inclinometer tilts caused by the azimuth-axis tilt are described as

$$\left.\begin{aligned} \alpha_{1x}(i) &= a\cos(e(i) + \varphi) \\ \alpha_{1y}(i) &= a\sin(e(i) + \varphi) \end{aligned}\right\} \tag{B-1}$$

or

$$\left.\begin{aligned} \alpha_{1x}(i) &= a_c c_i - a_s s_i \\ \alpha_{1y}(i) &= a_c s_i - a_s c_i \end{aligned}\right\} \tag{B-2}$$

where $a_c = a\cos(\varphi)$, $a_s = a\sin(\varphi)$, $c_i = \cos(e(i))$, and $s_i = \sin(e(i))$. For n samples, we define the following vectors and matrices:

$$\alpha_1 = \left\{ \begin{array}{c} \alpha_{1x} \\ \alpha_{1y} \end{array} \right\} \tag{B-3a}$$

where $\alpha_{1x} = \left\{ \begin{array}{c} \alpha_{1x}(1) \\ \alpha_{1x}(2) \\ \vdots \\ \alpha_{1x}(n) \end{array} \right\}$ and $\alpha_{1y} = \left\{ \begin{array}{c} \alpha_{1y}(1) \\ \alpha_{1y}(2) \\ \vdots \\ \alpha_{1y}(n) \end{array} \right\}$, and

$$P = \begin{bmatrix} c & -s \\ s & c \end{bmatrix} \tag{B-3b}$$

where $c = \begin{Bmatrix} c_1 \\ c_2 \\ \vdots \\ c_n \end{Bmatrix}$ and $s = \begin{Bmatrix} s_1 \\ s_2 \\ \vdots \\ s_n \end{Bmatrix}$, and

$$A = \begin{Bmatrix} a_c \\ a_s \end{Bmatrix} \tag{B-3c}$$

For the above notations, Eq .(B-2) can be rewritten in a compact form:

$$PA = \alpha_1 \tag{B-4}$$

The least-squares solution, A, of Eq. (B-4) is as follows:

$$A = (P^T P)^{-1} P^T \alpha_1 \tag{B-5}$$

But, from Eq. (B-3c), it follows that

$$\left.\begin{array}{l} a\cos(\varphi) = A_{11} \\ a\sin(\varphi) = A_{21} \end{array}\right\} \tag{B-6}$$

Therefore,

$$\left.\begin{array}{l} a = \sqrt{A_{11}^2 + A_{21}^2} \\ \varphi = \tan^{-1}\left(\dfrac{A_{21}}{A_{11}}\right) \end{array}\right\} \tag{B-7}$$